

Measurement of the ZZ cross-section in e^+e^- interactions at 183-189 GeV

DELPHI Collaboration

Abstract

Measurements of on-shell ZZ production are described, using data collected by DELPHI in 1997 and 1998, at centre-of-mass energies $\sqrt{s} = 182.6$ GeV and 188.6 GeV respectively. Results obtained in each of the final states $q\bar{q}q\bar{q}$, $\mu^+\mu^-q\bar{q}$, $e^+e^-q\bar{q}$, $\nu\bar{\nu}q\bar{q}$, $l^+l^-l^+l^-$, and $\nu\bar{\nu}l^+l^-$ are presented. The measured cross-sections for on-shell ZZ production via the tree-level doubly-resonant graphs (NC02) are:

$$\sigma_{NC02}(182.6 \text{ GeV}) = 0.38 \pm 0.18 \text{ (stat)} \pm 0.04 \text{ (syst)} \text{ pb},$$

$$\sigma_{NC02}(188.6 \text{ GeV}) = 0.60 \pm 0.13 \text{ (stat)} \pm 0.07 \text{ (syst)} \text{ pb}.$$

They are consistent with the Standard Model expectations of 0.25 pb and 0.65 pb at each energy.

(Accepted by Phys.Lett.B)

P.Abreu²², W.Adam⁵², T.Adye³⁸, P.Adzic¹², I.Ajinenko⁴⁴, Z.Albrecht¹⁸, T.Alderweireld², G.D.Alekseev¹⁷, R.Aleman⁹, T.Allmendinger¹⁸, P.P.Allport²³, S.Almehed²⁵, U.Amaldi²⁹, N.Amapane⁴⁷, S.Amato⁴⁹, E.G.Anassontzis³, P.Andersson⁴⁶, A.Andreazza²⁸, S.Andringa²², P.Antilogus²⁶, W-D.Apel¹⁸, Y.Arnoud¹⁵, B.Åsman⁴⁶, J-E.Augustin²⁴, A.Augustinus⁹, P.Baillon⁹, A.Ballestrero⁴⁷, P.Bambade^{9,20}, F.Barao²², G.Barbiellini⁴⁸, R.Barbier²⁶, D.Y.Bardin¹⁷, G.Barker¹⁸, A.Baroncelli⁴⁰, M.Battaglia¹⁶, M.Baubillier²⁴, K-H.Becks⁵⁴, M.Begalli⁶, A.Behrmann⁵⁴, P.Beilliere⁸, Yu.Belokopytov⁹, N.C.Benekos³³, A.C.Benvenuti⁵, C.Berat¹⁵, M.Berggren²⁴, L.Berntzon⁴⁶, D.Bertrand², M.Besancon⁴¹, M.S.Bilenky¹⁷, M-A.Bizouard²⁰, D.Bloch¹⁰, H.M.Blom³², M.Bonesini²⁹, M.Boonekamp⁴¹, P.S.L.Booth²³, G.Borisov²⁰, C.Bosio⁴³, O.Botner⁵⁰, E.Boudinov³², B.Bouquet²⁰, C.Bourdarios²⁰, T.J.V.Bowcock²³, I.Boyko¹⁷, I.Bozovic¹², M.Bozzo¹⁴, M.Bracko⁴⁵, P.Branchini⁴⁰, R.A.Brenner⁵⁰, P.Bruckman⁹, J-M.Brunet⁸, L.Bugge³⁴, T.Buran³⁴, P.Buschmann⁵⁴, S.Cabrera⁵¹, M.Caccia²⁸, M.Calvi²⁹, T.Camporesi⁹, V.Canale³⁹, F.Carena⁹, L.Carroll²³, C.Caso¹⁴, M.V.Castillo Gimenez⁵¹, A.Cattai⁹, F.R.Cavallo⁵, Ph.Charpentier⁹, P.Checchia³⁷, G.A.Chelkov¹⁷, R.Chierici⁴⁷, P.Chliapnikov^{9,44}, P.Chochula⁷, V.Chorowicz²⁶, J.Chudoba³¹, K.Cieslik¹⁹, P.Collins⁹, R.Contri¹⁴, E.Cortina⁵¹, G.Cosme²⁰, F.Cossutti⁹, M.Costa⁵¹, H.B.Crawley¹, D.Crennell³⁸, J.Croix¹⁰, J.Cuevas Maestro³⁵, S.Czellar¹⁶, J.D'Hondt², J.Dalmau⁴⁶, M.Davenport⁹, W.Da Silva²⁴, G.Della Ricca⁴⁸, P.Delpierre²⁷, N.Demaria⁴⁷, A.De Angelis⁴⁸, W.De Boer¹⁸, C.De Clercq², B.De Lotto⁴⁸, A.De Min⁹, L.De Paula⁴⁹, H.Dijkstra⁹, L.Di Ciaccio³⁹, J.Dolbeau⁸, K.Doroba⁵³, M.Dracos¹⁰, J.Drees⁵⁴, M.Dris³³, G.Eigen⁴, T.Ekelof⁵⁰, M.Ellert⁵⁰, M.Elsing⁹, J-P.Engel¹⁰, M.Espírito Santo⁹, G.Fanourakis¹², D.Fassouliotis¹², M.Feindt¹⁸, J.Fernandez⁴², A.Ferrer⁵¹, E.Ferrer-Ribas²⁰, F.Ferro¹⁴, A.Firestone¹, U.Flagmeyer⁵⁴, H.Foeth⁹, E.Fokitis³³, F.Fontanelli¹⁴, B.Franek³⁸, A.G.Frodesen⁴, R.Fruhwirth⁵², F.Fulda-Quenzer²⁰, J.Fuster⁵¹, A.Galloni²³, D.Gamba⁴⁷, S.Gamblin²⁰, M.Gandelman⁴⁹, C.Garcia⁵¹, C.Gaspar⁹, M.Gaspar⁴⁹, U.Gasparini³⁷, Ph.Gavillet⁹, E.N.Gazis³³, D.Gele¹⁰, T.Geralis¹², L.Gerdyukov⁴⁴, N.Ghodbane²⁶, I.Gil⁵¹, F.Glege⁵⁴, R.Gokieli^{9,53}, B.Golob^{9,45}, G.Gomez-Ceballos⁴², P.Goncalves²², I.Gonzalez Caballero⁴², G.Gopal³⁸, L.Gorn¹, Yu.Gouz⁴⁴, V.Gracco¹⁴, J.Grahl¹, E.Graziani⁴⁰, P.Gris⁴¹, G.Grosdidier²⁰, K.Grzelak⁵³, J.Guy³⁸, C.Haag¹⁸, F.Hahn⁹, S.Hahn⁵⁴, S.Haider⁹, A.Hallgren⁵⁰, K.Hamacher⁵⁴, J.Hansen³⁴, F.J.Harris³⁶, S.Haug³⁴, F.Hauler¹⁸, V.Hedberg^{9,25}, S.Heising¹⁸, J.J.Hernandez⁵¹, P.Herquet², H.Herr⁹, E.Higon⁵¹, S-O.Holmgren⁴⁶, P.J.Holt³⁶, S.Hoorelbeke², M.Houlden²³, J.Hrube⁵², M.Huber¹⁸, G.J.Hughes²³, K.Hultqvist^{9,46}, J.N.Jackson²³, R.Jacobsson⁹, P.Jalocha¹⁹, R.Janik⁷, Ch.Jarlskog²⁵, G.Jarlskog²⁵, P.Jarry⁴¹, B.Jean-Marie²⁰, D.Jeans³⁶, E.K.Johansson⁴⁶, P.Jonsson²⁶, C.Joram⁹, P.Juillot¹⁰, L.Jungermann¹⁸, F.Kapusta²⁴, K.Karafasoulis¹², S.Katsanevas²⁶, E.C.Katsoufis³³, R.Keranen¹⁸, G.Kernel⁴⁵, B.P.Kersevan⁴⁵, Yu.Khokhlov⁴⁴, B.A.Khomenko¹⁷, N.N.Khovanski¹⁷, A.Kiiskinen¹⁶, B.King²³, A.Kinvig²³, N.J.Kjaer⁹, O.Klapp⁵⁴, P.Kluit³², P.Kokkinias¹², V.Kostioukhine⁴⁴, C.Kourkoumelis³, O.Kouznetsov¹⁷, M.Krammer⁵², E.Kriznic⁴⁵, Z.Krumstein¹⁷, P.Kubinec⁷, J.Kurowska⁵³, K.Kurvinen¹⁶, J.W.Lamsa¹, D.W.Lane¹, J-P.Laugier⁴¹, R.Lauhakangas¹⁶, G.Leder⁵², F.Ledroit¹⁵, L.Leinonen⁴⁶, A.Leisos¹², R.Leitner³¹, J.Lemonne², G.Lenzen⁵⁴, V.Lepeltier²⁰, T.Lesiak¹⁹, M.Lethuillier²⁶, J.Libby³⁶, W.Liebig⁵⁴, D.Liko⁹, A.Lipniacka⁴⁶, I.Lippi³⁷, B.Loerstad²⁵, J.G.Loken³⁶, J.H.Lopes⁴⁹, J.M.Lopez⁴², R.Lopez-Fernandez¹⁵, D.Loukas¹², P.Lutz⁴¹, L.Lyons³⁶, J.MacNaughton⁵², J.R.Mahon⁶, A.Mai²², A.Malek⁵⁴, S.Maltezos³³, V.Malychev¹⁷, F.Mandl⁵², J.Marco⁴², R.Marco⁴², B.Marechal⁴⁹, M.Margoni³⁷, J-C.Marin⁹, C.Mariotti⁹, A.Markou¹², C.Martinez-Rivero⁹, S.Marti i Garcia⁹, J.Masik¹³, N.Mastroiannopoulos¹², F.Matorras⁴², C.Matteuzzi²⁹, G.Matthiae³⁹, F.Mazzucato³⁷, M.Mazzucato³⁷, M.Mc Cubbin²³, R.Mc Kay¹, R.Mc Nulty²³, G.Mc Pherson²³, E.Merle¹⁵, C.Meroni²⁸, W.T.Meyer¹, E.Migliore⁹, L.Mirabito²⁶, W.A.Mitaroff⁵², U.Mjoernmark²⁵, T.Moa⁴⁶, M.Moch¹⁸, R.Moeller³⁰, K.Moenig^{9,11}, M.R.Monge¹⁴, J.Montenegro³², D.Moraes⁴⁹, P.Morettini¹⁴, G.Morton³⁶, U.Mueller⁵⁴, K.Muenich⁵⁴, M.Mulders³², C.Mulet-Marquis¹⁵, L.M.Mundim⁶, R.Muresan²⁵, W.J.Murray³⁸, B.Muryn¹⁹, G.Myatt³⁶, T.Myklebust³⁴, F.Naraghi¹⁵, M.Nassiakou¹², F.L.Navarria⁵, K.Nawrocki⁵³, P.Negri²⁹, N.Neufeld⁵², R.Nicolaidou⁴¹, B.S.Nielsen³⁰, P.Niezurawski⁵³, M.Nikolenko^{10,17}, V.Nomokonov¹⁶, A.Nygren²⁵, V.Obraztsov⁴⁴, A.G.Olshevski¹⁷, A.Onofre²², R.Orava¹⁶, K.Osterberg⁹, A.Ouraou⁴¹, A.Oyanguren⁵¹, M.Paganoni²⁹, S.Paiano⁵, R.Pain²⁴, R.Paiva²², J.Palacios³⁶, H.Palka¹⁹, Th.D.Papadopoulou³³, L.Pape⁹, C.Parkes⁹, F.Parodi¹⁴, U.Parzefall²³, A.Passerì⁴⁰, O.Passon⁵⁴, T.Pavel²⁵, M.Pegoraro³⁷, L.Peralta²², M.Pernicka⁵², A.Perrotta⁵, C.Petridou⁴⁸, A.Petrolini¹⁴, H.T.Phillips³⁸, F.Pierre⁴¹, M.Pimenta²², E.Piotto²⁸, T.Podobnik⁴⁵, V.Poireau⁴¹, M.E.Pol⁶, G.Polok¹⁹, P.Poropat⁴⁸, V.Pozdniakov¹⁷, P.Privitera³⁹, N.Pukhaeva¹⁷, A.Pullia²⁹, D.Radojicic³⁶, S.Ragazzi²⁹, H.Rahmani³³, J.Rames¹³, P.N.Ratoff²¹, A.L.Read³⁴, P.Rebecchi⁹, N.G.Redaeli²⁹, M.Regler⁵², J.Rehn¹⁸, D.Reid³², P.Reinertsen⁴, R.Reinhardt⁵⁴, P.B.Renton³⁶, L.K.Resvanis³, F.Richard²⁰, J.Ridky¹³, G.Rinaudo⁴⁷, I.Ripp-Baudot¹⁰, A.Romero⁴⁷, P.Ronchese³⁷, E.I.Rosenberg¹, P.Rosinsky⁷, P.Roudeau²⁰, T.Rovelli⁵, V.Ruhlmann-Kleider⁴¹, A.Ruiz⁴², H.Saarikko¹⁶, Y.Sacquin⁴¹, A.Sadovsky¹⁷, G.Sajot¹⁵, J.Salt⁵¹, D.Sampsonidis¹², M.Sannino¹⁴, A.Savoy-Navarro²⁴, C.Schwanda⁵², Ph.Schwemling²⁴, B.Schwering⁵⁴, U.Schwickerath¹⁸, F.Scuri⁴⁸, P.Seager²¹, Y.Sedykh¹⁷, A.M.Segar³⁶, N.Seibert¹⁸, R.Sekulin³⁸, G.Sette¹⁴, R.C.Shellard⁶, M.Siebel⁵⁴, L.Simard⁴¹, F.Simonetto³⁷, A.N.Sisakian¹⁷, G.Smadja²⁶, N.Smirnov⁴⁴, O.Smirnova²⁵, G.R.Smith³⁸, A.Sokolov⁴⁴, O.Solovianov⁴⁴, A.Sopczak¹⁸, R.Sosnowski⁵³, T.Spaso⁹, E.Spiriti⁴⁰, S.Squarcia¹⁴, C.Stanescu⁴⁰, M.Stanitzki¹⁸, K.Stevenson³⁶, A.Stocchi²⁰, J.Strauss⁵², R.Strub¹⁰, B.Stugu⁴, M.Szczekowski⁵³, M.Szeptycka⁵³, T.Tabarelli²⁹, A.Taffard²³, F.Tegenfeldt⁵⁰, F.Terranova²⁹, J.Timmermans³², N.Tinti⁵, L.G.Tkatchev¹⁷, M.Tobin²³, S.Todorova⁹, B.Tome²², A.Tonazzo⁹, L.Tortora⁴⁰, P.Tortosa⁵¹, G.Transtomer²⁵, D.Treille⁹, G.Tristram⁸, M.Trochimczuk⁵³, C.Troncon²⁸, M-L.Turluer⁴¹, I.A.Tyapkin¹⁷, P.Tyapkin²⁵, S.Tzamarias¹², O.Ullaland⁹, V.Uvarov⁴⁴, G.Valenti^{9,5}, E.Vallazza⁴⁸, P.Van Dam³², W.Van den Boeck², W.K.Van Doninck²,

J. Van Eldik^{9,32}, A. Van Lysebetten², N. van Remortel², I. Van Vulpen³², G. Vegni²⁸, L. Ventura³⁷, W. Venus^{38,9}, F. Verbeure², P. Verdier²⁶, M. Verlato³⁷, L. S. Vertogradov¹⁷, V. Verzi²⁸, D. Vilanova⁴¹, L. Vitale⁴⁸, E. Vlasov⁴⁴, A. S. Vodopyanov¹⁷, G. Voulgaris³, V. Vrba¹³, H. Wahlen⁵⁴, A. J. Washbrook²³, C. Weiser⁹, D. Wicke⁹, J. H. Wickens², G. R. Wilkinson³⁶, M. Winter¹⁰, M. Witek¹⁹, G. Wolf⁹, J. Yi¹, O. Yushchenko⁴⁴, A. Zalewska¹⁹, P. Zalewski⁵³, D. Zavrtnik⁴⁵, E. Zevgolatakos¹², N. I. Zimin^{17,25}, A. Zintchenko¹⁷, Ph. Zoller¹⁰, G. Zumerle³⁷, M. Zupan¹²

¹Department of Physics and Astronomy, Iowa State University, Ames IA 50011-3160, USA

²Physics Department, Univ. Instelling Antwerpen, Universiteitsplein 1, B-2610 Antwerpen, Belgium and IIHE, ULB-VUB, Pleinlaan 2, B-1050 Brussels, Belgium and Faculté des Sciences, Univ. de l'Etat Mons, Av. Maistriau 19, B-7000 Mons, Belgium

³Physics Laboratory, University of Athens, Solonos Str. 104, GR-10680 Athens, Greece

⁴Department of Physics, University of Bergen, Allégaten 55, NO-5007 Bergen, Norway

⁵Dipartimento di Fisica, Università di Bologna and INFN, Via Irnerio 46, IT-40126 Bologna, Italy

⁶Centro Brasileiro de Pesquisas Físicas, rua Xavier Sigaud 150, BR-22290 Rio de Janeiro, Brazil and Depto. de Física, Pont. Univ. Católica, C.P. 38071 BR-22453 Rio de Janeiro, Brazil and Inst. de Física, Univ. Estadual do Rio de Janeiro, rua São Francisco Xavier 524, Rio de Janeiro, Brazil

⁷Comenius University, Faculty of Mathematics and Physics, Mlynska Dolina, SK-84215 Bratislava, Slovakia

⁸Collège de France, Lab. de Physique Corpusculaire, IN2P3-CNRS, FR-75231 Paris Cedex 05, France

⁹CERN, CH-1211 Geneva 23, Switzerland

¹⁰Institut de Recherches Subatomiques, IN2P3 - CNRS/ULP - BP20, FR-67037 Strasbourg Cedex, France

¹¹Now at DESY-Zeuthen, Platanenallee 6, D-15735 Zeuthen, Germany

¹²Institute of Nuclear Physics, N.C.S.R. Demokritos, P.O. Box 60228, GR-15310 Athens, Greece

¹³FZU, Inst. of Phys. of the C.A.S. High Energy Physics Division, Na Slovance 2, CZ-180 40, Praha 8, Czech Republic

¹⁴Dipartimento di Fisica, Università di Genova and INFN, Via Dodecaneso 33, IT-16146 Genova, Italy

¹⁵Institut des Sciences Nucléaires, IN2P3-CNRS, Université de Grenoble 1, FR-38026 Grenoble Cedex, France

¹⁶Helsinki Institute of Physics, HIP, P.O. Box 9, FI-00014 Helsinki, Finland

¹⁷Joint Institute for Nuclear Research, Dubna, Head Post Office, P.O. Box 79, RU-101 000 Moscow, Russian Federation

¹⁸Institut für Experimentelle Kernphysik, Universität Karlsruhe, Postfach 6980, DE-76128 Karlsruhe, Germany

¹⁹Institute of Nuclear Physics and University of Mining and Metallurgy, Ul. Kawiora 26a, PL-30055 Krakow, Poland

²⁰Université de Paris-Sud, Lab. de l'Accélérateur Linéaire, IN2P3-CNRS, Bât. 200, FR-91405 Orsay Cedex, France

²¹School of Physics and Chemistry, University of Lancaster, Lancaster LA1 4YB, UK

²²LIP, IST, FCUL - Av. Elias Garcia, 14-1º, PT-1000 Lisboa Codex, Portugal

²³Department of Physics, University of Liverpool, P.O. Box 147, Liverpool L69 3BX, UK

²⁴LPNHE, IN2P3-CNRS, Univ. Paris VI et VII, Tour 33 (RdC), 4 place Jussieu, FR-75252 Paris Cedex 05, France

²⁵Department of Physics, University of Lund, Sölvegatan 14, SE-223 63 Lund, Sweden

²⁶Université Claude Bernard de Lyon, IPNL, IN2P3-CNRS, FR-69622 Villeurbanne Cedex, France

²⁷Univ. d'Aix - Marseille II - CPP, IN2P3-CNRS, FR-13288 Marseille Cedex 09, France

²⁸Dipartimento di Fisica, Università di Milano and INFN-MILANO, Via Celoria 16, IT-20133 Milan, Italy

²⁹Dipartimento di Fisica, Univ. di Milano-Bicocca and INFN-MILANO, Piazza delle Scienze 2, IT-20126 Milan, Italy

³⁰Niels Bohr Institute, Blegdamsvej 17, DK-2100 Copenhagen Ø, Denmark

³¹IPNP of MFF, Charles Univ., Areal MFF, V Holesovickach 2, CZ-180 00, Praha 8, Czech Republic

³²NIKHEF, Postbus 41882, NL-1009 DB Amsterdam, The Netherlands

³³National Technical University, Physics Department, Zografou Campus, GR-15773 Athens, Greece

³⁴Physics Department, University of Oslo, Blindern, NO-1000 Oslo 3, Norway

³⁵Dpto. Física, Univ. Oviedo, Avda. Calvo Sotelo s/n, ES-33007 Oviedo, Spain

³⁶Department of Physics, University of Oxford, Keble Road, Oxford OX1 3RH, UK

³⁷Dipartimento di Fisica, Università di Padova and INFN, Via Marzolo 8, IT-35131 Padua, Italy

³⁸Rutherford Appleton Laboratory, Chilton, Didcot OX11 0QX, UK

³⁹Dipartimento di Fisica, Università di Roma II and INFN, Tor Vergata, IT-00173 Rome, Italy

⁴⁰Dipartimento di Fisica, Università di Roma III and INFN, Via della Vasca Navale 84, IT-00146 Rome, Italy

⁴¹DAPNIA/Service de Physique des Particules, CEA-Saclay, FR-91191 Gif-sur-Yvette Cedex, France

⁴²Instituto de Física de Cantabria (CSIC-UC), Avda. los Castros s/n, ES-39006 Santander, Spain

⁴³Dipartimento di Fisica, Università degli Studi di Roma La Sapienza, Piazzale Aldo Moro 2, IT-00185 Rome, Italy

⁴⁴Inst. for High Energy Physics, Serpukov P.O. Box 35, Protvino, (Moscow Region), Russian Federation

⁴⁵J. Stefan Institute, Jamova 39, SI-1000 Ljubljana, Slovenia and Laboratory for Astroparticle Physics, Nova Gorica Polytechnic, Kostanjevska 16a, SI-5000 Nova Gorica, Slovenia, and Department of Physics, University of Ljubljana, SI-1000 Ljubljana, Slovenia

⁴⁶Fysikum, Stockholm University, Box 6730, SE-113 85 Stockholm, Sweden

⁴⁷Dipartimento di Fisica Sperimentale, Università di Torino and INFN, Via P. Giuria 1, IT-10125 Turin, Italy

⁴⁸Dipartimento di Fisica, Università di Trieste and INFN, Via A. Valerio 2, IT-34127 Trieste, Italy and Istituto di Fisica, Università di Udine, IT-33100 Udine, Italy

⁴⁹Univ. Federal do Rio de Janeiro, C.P. 68528 Cidade Univ., Ilha do Fundão BR-21945-970 Rio de Janeiro, Brazil

⁵⁰Department of Radiation Sciences, University of Uppsala, P.O. Box 535, SE-751 21 Uppsala, Sweden

⁵¹IFIC, Valencia-CSIC, and D.F.A.M.N., U. de Valencia, Avda. Dr. Moliner 50, ES-46100 Burjassot (Valencia), Spain

⁵²Institut für Hochenergiephysik, Österr. Akad. d. Wissensch., Nikolsdorfergasse 18, AT-1050 Vienna, Austria

⁵³Inst. Nuclear Studies and University of Warsaw, Ul. Hoza 69, PL-00681 Warsaw, Poland

⁵⁴Fachbereich Physik, University of Wuppertal, Postfach 100 127, DE-42097 Wuppertal, Germany

1 Introduction

The study of doubly resonant production of Z bosons is a relatively new topic. The first evidence [1] was accumulated during 1997, when LEP was operated at a centre-of-mass energy of 182.6 GeV, corresponding to the threshold for this channel. In this letter we present measurements of the production cross-section both from that run and from the 1998 run at 188.6 GeV.

There are several motivations for studying this channel. Firstly, it is necessary to check that the observed production rate of any expected physical process seen for the first time in a new energy domain is well accounted for by the Standard Model. Deviations from predictions could be interpreted as a signal for new physics beyond the Standard Model, manifesting itself through anomalous production [2,3], for instance by means of anomalous neutral-current triple gauge boson couplings [4]. Secondly, ZZ production forms an irreducible background to the Higgs search at LEP when the mass of the Higgs boson is close to that of the Z [5]. In this context the results obtained also give some indication of the reliability of the techniques used in the Higgs search.

In what follows, the data sets and simulations used are described and the signal definition which was adopted is discussed. The event selections developed in the six sub-channels which were analysed are then presented. Results are given in the form of a comparison of the numbers of found and predicted selected events, together with an evaluation of the main systematic effects. Finally, the combination of the sub-channel results into overall ZZ cross-sections is described and the overall measurements are compared to the Standard Model expectation.

2 Data samples

DELPHI took data at centre-of-mass energies of 182.6 GeV in 1997 and 188.6 GeV in 1998, with integrated luminosities of 54 pb⁻¹ and 158 pb⁻¹ respectively. A detailed description of the detector and a review of its performance can be found in [6,7]. The detector was not changed in recent years, except for upgrades of the vertex detector [8], and the addition of a set of scintillator counters to veto photons in blind regions of the electromagnetic calorimetry, at polar angles near 40° and 90°.

Simulated events were produced with the DELPHI simulation program DELSIM[7] and were then passed through the same reconstruction and analysis chain as the data. The generation of processes leading to four-fermion final states was done with EXCALIBUR[9], relying on JETSET 7.4 [10] for quark fragmentation. GRC4F[11] was used as a complementary generator for four-fermion final states resulting from $W e \nu_e$ processes when $\cos \theta_e > 0.9999$. Two fermion processes $e^+e^- \rightarrow f\bar{f}(+n\gamma)$ were generated using PYTHIA [10], $e^+e^- \rightarrow \mu^+\mu^-(+n\gamma)$ and $e^+e^- \rightarrow \tau^+\tau^-(+n\gamma)$ with KORALZ[12], and $e^+e^- \rightarrow e^+e^-(+n\gamma)$ with BHWIDE[13]. Two-photon interactions were generated using TWOGAM [14] and BDK [15].

3 Signal definition

The region of phase-space at high di-fermion masses must be isolated to measure the ZZ production cross-section. In order to interpret the measurement in terms of the tree-level doubly-resonant graphs shown in Figure 1 (referred to as the NC02 graphs) the presence of other four-fermion processes in this region must be taken into account. For this purpose the signal was defined in the simulation by requiring that the generated

masses of the two appropriate pairings of final-state fermions be within $10 \text{ GeV}/c^2$ of the nominal Z mass. This choice of mass window maximized the sensitivity to the NC02 graphs while minimizing contributions from other four-fermion processes. Events with the correct flavour composition but which fell outside this generator-level mass window were considered as background. A scaling factor R ,

$$R = \frac{\sigma_{\text{NC02}}^{\text{total}}}{\sigma_{4f}^{\text{window}}}, \quad (1)$$

was then calculated at generator level to enable conversion of the measured total four-fermion cross-section within the mass window, $\sigma_{4f}^{\text{window}}$, into the total NC02 cross-section, $\sigma_{\text{NC02}}^{\text{total}}$. The scaling factors obtained for each channel are shown in table 1. Most of the values are close to unity, confirming that the defined region is dominated by on-shell ZZ production. Several sources of bias which could result from this procedure were investigated. The most relevant among these were:

- In the channel $e^+e^-q\bar{q}$, the scaling factors are smaller than unity. This arises because of significant contributions from the single-resonant process e^+e^-Z . Since the electrons from this process tend to be peaked in the forward directions and since the efficiencies to identify electrons are reduced in these regions, there is a bias for this particular channel from taking a scaling factor averaged over the full solid angle. The magnitude of this bias was estimated by computing the expected cross-sections using this procedure in the barrel and forward regions separately. A 2.75% correction was derived and incorporated into the scaling factor quoted in table 1.
- In the channel $l^+l^-l^+l^-$ the factor is significantly smaller than unity. This arises because of the intrinsic ambiguity in pairing, existing in cases with four leptons of the same family, for which there are significant contributions in the signal window from $Z\gamma^*$ processes. As an additional cross-check for this channel the measurement was also repeated using an additive correction procedure (see the corresponding section), yielding fully consistent results.

Final State	183 GeV	189 GeV
$q\bar{q}q\bar{q}$	1.26	1.07
$\nu\bar{\nu}q\bar{q}$	1.14	1.05
$\mu^+\mu^-q\bar{q}$	1.19	1.05
$e^+e^-q\bar{q}$	0.83	0.88
$l^+l^-l^+l^-$	0.46	0.59
$\nu\bar{\nu}l^+l^-$	1.00	1.00

Table 1: Scaling factors R computed at generator level to convert the measured total four-fermion cross-section within the signal defining mass window $|M_{f\bar{f}} - M_Z| < 10 \text{ GeV}/c^2$, $\sigma_{4f}^{\text{window}}$, into the total NC02 cross-section, $\sigma_{\text{NC02}}^{\text{total}}$.

4 Four jets

The $ZZ \rightarrow q\bar{q}q\bar{q}$ process represents 49% of the ZZ final states and results typically in events with four or more jets. The principal backgrounds arise from WW and $q\bar{q}(\gamma)$ processes, which can lead to similar multijet topologies. The main ingredients used

to isolate the signal were the b -tagging of the jets, topological information quantifying their separation, and reconstructed di-jet masses. A pre-selection was first applied to isolate hadronic events with at least four reconstructed jets, as in [16]. Four and five jet events were treated separately throughout the analysis¹.

In order to optimally use the information from the b -tagging, the ratio of the distributions of the combined b -tagging variable [17] for b and non- b jets were parametrized in three different angular regions, using simulated Z decays. Using these parametrisations and the measured value of the combined b -tagging variable for each jet, the probability that it originated from the fragmentation of a b or a non- b quark was evaluated.

In order to fully exploit the information from the mass reconstruction, all possible di-jet pairings were used, following the method outlined in [16]. For each of the physics hypotheses ZZ , WW and $q\bar{q}(\gamma)$, the expected probability distributions for the different mass combinations in an event were expressed in analytical form, by means of products of Breit-Wigners and phase-space factors for the correctly paired mass combinations in WW and ZZ events, and of flat spectra for all the other cases. Using the event-by-event jet errors, measured χ^2 probability distributions were obtained, as functions of the possible di-jet masses, by kinematic fits [18] requiring four-momentum conservation and equality of each di-jet mass with the tested value. These two-dimensional measurement probabilities were then convoluted with the expected distributions to quantify the compatibility of each pairing with the ZZ , WW and $q\bar{q}(\gamma)$ hypotheses from the mass information alone.

Finally the topological variable $E_{\min} \cdot \alpha_{\min}$ was defined, where E_{\min} is the minimum jet-energy and α_{\min} the minimum opening angle between any jet pair. The ratio of two-fermion and four-fermion events was parametrized as a function of this variable using simulated data for four- and five-jet events separately.

Looking for all possible hadronic ZZ final states and using the predicted SM cross-sections and branching ratios into the different quark configurations, the b -like probability per jet, the topological information per event and the mass information per pairing, a combined variable quantifying the compatibility of any event with the ZZ hypothesis was constructed. This combined variable was shown to behave as a genuine probability for the ZZ hypothesis, and provided high discriminating power. The distribution of this variable at 188.6 GeV is shown in Figure 2. Results obtained by cutting on this variable are presented in table 2.

182.6 GeV	data	Total MC	ZZ	$Z\gamma^*$	WW	$q\bar{q}(\gamma)$
After pre-selection	535	510.8	6.73	7.06	336.2	160.8
At maximum $\epsilon \cdot p$	2	1.68	1.01	0.10	0.11	0.46

188.6 GeV	data	Total MC	ZZ	$Z\gamma^*$	WW	$q\bar{q}(\gamma)$
After pre-selection	1538	1536.0	41.8	17.7	1039.6	437.0
At maximum $\epsilon \cdot p$	42	43.06	15.54	1.41	16.01	10.10
At $S/B = 2.92$	7	7.69	5.73	0.38	0.28	1.30

Table 2: The observed and expected number of selected events after the pre-selection at 182.6 GeV and at 188.6 GeV, for integrated luminosities of 53 pb^{-1} and 158 pb^{-1} respectively. The two last lines give the number of events left at the maximum of efficiency \times purity ($\epsilon \cdot p$) and at a signal-to-background ratio, S/B , of about 3.

¹Events with more than five reconstructed jets were forced into a five-jet configuration.

Systematic effects resulting from uncertainties in signal efficiency, in the conversion factor to translate the results to a NC02 cross-section and in the predicted background level were studied. The largest errors came from uncertainties in the modeling of multijet $q\bar{q}(\gamma)$ processes with b quarks composing the main remaining background, and from the sensitivity of the b -tagging procedure to the jet multiplicity. The dominant $q\bar{q}(\gamma)$ modeling uncertainty came from the limited precision with which the $g \rightarrow b\bar{b}$ rate is known, and to a lesser extent from uncertainties in the amount of reduction in gluon radiation off b quarks (also known as the dead-cone effect). These uncertainties, as well as biases in the treatments provided by the generator, have been studied [19] by comparing results of analytic calculations with dedicated measurements at LEP-1 and with predictions of the generators used in the simulation. Uncertainties in selection efficiencies related to the b -tagging procedure were studied by comparing efficiencies for two and four jet events at LEP-1 energies. By propagating effects from these sources into the analysis, a combined systematic uncertainty of around 6% was estimated relative to the expected cross-section.

5 Jets and a pair of isolated leptons

The decay modes $e^+e^- \rightarrow \mu^+\mu^-q\bar{q}$ and $e^+e^- \rightarrow e^+e^-q\bar{q}$ represent 9% of the ZZ final states. Events with $\tau^+\tau^-$ pairs were not considered. The two final state leptons are typically well isolated from all other particles. This can be used to select such events with high efficiency in both the muon and electron channels. Events were selected initially without explicit cuts on the masses of the final state fermion pairs in order to analyse simultaneously ZZ , $Z\gamma^*$ events and contributions from other possible diagrams leading to final states such as Ze^+e^- or t-channel γ^* exchange with Z/γ -strahlung. Mass cuts were then applied to isolate the ZZ contribution.

A loose hadronic pre-selection was first applied, requiring that events have at least 7 charged particles and a charged energy above $0.30 \sqrt{s}$. To suppress the radiative return to the Z boson, events were rejected if a photon with energy more than 60 GeV was found. The selection procedures then proceeded in a closely similar way for both $\mu^+\mu^-q\bar{q}$ and $e^+e^-q\bar{q}$ channels. In order to maximize the lepton identification efficiency, any charged particle with a momentum exceeding 5 GeV/c was considered as a possible lepton candidate around which nearby photons, if present, could be clustered. This was found to be necessary to improve the energy evaluation in the presence of final state radiation, and, in the case of electrons, bremsstrahlung. In the case of the $e^+e^-q\bar{q}$ channel, photons with energy between 20 GeV and 60 GeV were also considered as electron candidates, to recover events in which the electron track was not reconstructed.

Events with at least two lepton candidates of the same flavour, opposite charge and invariant mass exceeding $2 \text{ GeV}/c^2$ were then selected. All particles except the lepton candidates were clustered into jets and a kinematic fit requiring four-momentum conservation was applied, correcting appropriately the errors on lepton energies in cases where photons had been added by the clustering procedure.

At least one of the two lepton candidates was required to satisfy strong lepton identification criteria, while softer requirements were specified for the second. Muons were considered as strongly identified if selected by the standard DELPHI muon identification package [7], based mainly on finding associated hits in the muon chambers. For soft muon identification only a set of kinematic and calorimetric criteria were used. Electrons were considered as strongly identified when the energy deposited in the electromagnetic calorimeter exceeded 60% of the cluster energy or 15 GeV and when the energy deposited in the hadron calorimeter was reasonably limited. For soft electron identification only

requirements on the momentum of the charged particle in the cluster and on the energy deposited in the hadron calorimeter were used. Moreover electron candidates originating from applying the clustering procedure around a photon were considered as softly identified.

Two discriminating variables were then defined for final event selection: P_t^{min} , the lesser of the transverse momenta of the lepton candidates with respect to their nearest jet and the χ^2 per degree of freedom of the kinematic fit. The distribution of the mass of one fermion pair (l^+l^- or $q\bar{q}$) when the mass of the second pair is within 15 GeV/c² of the nominal Z mass is shown in figure 3a,b. The distribution of the sum of masses of two fermion pairs is shown in figure 3c. The observed distributions are in reasonable agreement with the predictions from simulation. To select on-shell ZZ production, cuts were placed simultaneously on the masses of the l^+l^- pair, on the remaining hadron system, and on their sum, taking into account in the performance optimization the different mass resolutions of these final states and the presence of the single-resonant process, e^+e^-Z in the case of the $e^+e^-q\bar{q}$ channel. The observed and predicted numbers of selected events are shown in table 3. The background is divided into two parts: the first one comes from $l^+l^-q\bar{q}$ events outside the generation-level signal window, and the second one comes from other processes, principally W^+W^- , other ZZ decays and (in the case of $e^+e^-q\bar{q}$) $q\bar{q}(+\gamma)$ production. For the $\mu^+\mu^-q\bar{q}$ channel, the efficiencies of the selection were 0.89 ± 0.02 and 0.86 ± 0.01 at 182.6 and 188.6 GeV respectively. For the $e^+e^-q\bar{q}$ channel, they were 0.73 ± 0.03 and 0.72 ± 0.02 respectively.

E_{cms} GeV	channel	data	Total MC	MC signal	MC $l^+l^-q\bar{q}$ backgr.	MC other backgr.
182.6	$\mu^+\mu^-q\bar{q}$	3	0.52 ± 0.03	0.48 ± 0.03	0.04 ± 0.01	0.00 ± 0.01
	$e^+e^-q\bar{q}$	0	0.69 ± 0.07	0.55 ± 0.05	0.10 ± 0.02	0.04 ± 0.04
	Total	3	1.21 ± 0.08	1.03 ± 0.06	0.14 ± 0.02	0.04 ± 0.04
188.6	$\mu^+\mu^-q\bar{q}$	5	4.15 ± 0.11	3.92 ± 0.10	0.19 ± 0.02	0.04 ± 0.03
	$e^+e^-q\bar{q}$	3	4.04 ± 0.15	3.55 ± 0.13	0.35 ± 0.04	0.14 ± 0.06
	Total	8	8.19 ± 0.19	7.47 ± 0.16	0.54 ± 0.04	0.18 ± 0.07
All	$\mu^+\mu^-q\bar{q}$	8	4.67 ± 0.11	4.40 ± 0.11	0.23 ± 0.02	0.04 ± 0.03
	$e^+e^-q\bar{q}$	3	4.73 ± 0.17	4.10 ± 0.14	0.45 ± 0.05	0.18 ± 0.07
	Total	11	9.40 ± 0.20	8.50 ± 0.18	0.68 ± 0.05	0.22 ± 0.08

Table 3: The observed and expected number of selected $l^+l^-q\bar{q}$ events - candidates to the on-shell ZZ production. The errors shown are due to the simulation statistics only. The expected numbers of the signal events are for the SM cross-section of the on-shell ZZ production.

Several sources of systematic errors were investigated. Uncertainties in the lepton identification were estimated comparing semileptonic W^+W^- events selected in data and simulation using the strong lepton identification criteria. Uncertainties in signal efficiencies from the description of the kinematic observables used were evaluated comparing the P_t and χ^2 distributions in data and simulation for all $l^+l^-q\bar{q}$ events selected without mass cuts. Corresponding uncertainties in background levels were evaluated by comparing samples of events selected in data and in simulation requiring both isolated tracks not to be identified as leptons, while maintaining all other criteria. Finally, uncertainties in the background level in the $e^+e^-q\bar{q}$ channel from fake electrons were studied with $Z\gamma$

events selected in data and in simulation with purely kinematic criteria. Propagating the found differences to the final stage of the analysis yielded a combined systematic error on the efficiency to select $l^+l^-q\bar{q}$ events of $\pm 3.0\%$. The uncertainty resulting for the background level amounted to about $\pm 15\%$.

6 Jets and missing energy

The decay mode $\nu\bar{\nu}q\bar{q}$ represents 28% of the ZZ final states. Its signature is a pair of jets relatively acoplanar with the beam and with visible and recoil masses compatible with the Z mass. The most difficult backgrounds arise from single resonant $We\nu_e$ processes, from WW processes where one of the W decays into $\tau\nu_\tau$, and from $q\bar{q}$ events, accompanied or not by isolated photons escaping detection, in which one or two of the jets were badly reconstructed.

A pre-selection was first applied to remove the bulk of the background. Multihadronic annihilation events were selected by requiring that the number of charged particles be larger than 8, that the track of at least one charged particle, with a transverse momentum larger than 1.5 GeV/c, extrapolate back to within 200 μm of the primary vertex in the plane transverse to the beam axis, that the total charged energy of the event exceed 10% of the centre-of-mass energy and that its raw visible mass be in the range $81 \pm 22 \text{ GeV}/c^2$. To reject radiative returns to the Z with energetic photons emitted in blind regions of the electromagnetic calorimetry (at polar angles near 40° and 90°) signals from dedicated scintillator counters were used.

A combined discriminant variable was then constructed using the Iterative Discriminant Analysis program (IDA) [20] to calculate a second order polynomial from seven event variables, selected based on their discriminating power and independence:

- The minimum polar angle defining a cone in the positive and negative beam directions containing 15% of the total visible energy.
- The logarithm of the acoplanarity scaled by the sine of the minimum polar angle between a jet direction and the beam axis.
- The total reconstructed energy.
- The maximum transverse momentum between any particle and a jet.
- The energy of the more energetic among the reconstructed jets.
- The thrust, computed in the rest frame of the visible system.
- The acollinearity of the jets.

Moreover, to concentrate on the signal region when optimizing the second-order discriminant function, very loose cuts were applied on these variables, at values corresponding to the tails of the signal distributions and removing each about one percent of it. Finally, the total energy of hypothetical photons escaping in the beam direction was estimated from the two jet directions and was required to be less than 85% of the value expected for radiative returns to the Z .

The comparison of selected data and simulation rates for the signal and background components is shown in Figure 4a (for the 188.6 GeV data) and in table 4. The ZZ cross-section at each energy was obtained from a binned maximum likelihood fit of this discriminant output with the ZZ signal contribution as the only free parameter.

At both energies more events than predicted were observed before the final selections. This resulted mainly from uncertainties in the description of the energy reconstruction of the $q\bar{q}(\gamma)$ background. Unlike the other ZZ decay channels studied, in which the

183 GeV	Data	Total MC	Signal	CC 4-f	$q\bar{q}\gamma$	$q\bar{q}l^+l^-$	$\gamma\gamma$
After pre-selection	2485	2286 ± 10	3.5 ± 0.1	134 ± 1	2005 ± 4	6.9 ± 0.2	137 ± 9
After tail cuts	235	209 ± 2	3.0 ± 0.1	37 ± 0.6	163 ± 1	1.0 ± 0.1	5.1 ± 1.6
After final DA cut	22	21.9 ± 0.45	2.4 ± 0.1	8.8 ± 0.3	10.6 ± 0.4	0.07 ± 0.03	0
189 GeV	Data	Total MC	Signal	CC 4-f	$q\bar{q}\gamma$	$q\bar{q}l^+l^-$	$\gamma\gamma$
After pre-selection	6723	6206 ± 20	21.5 ± 0.3	344 ± 2	5344 ± 7	17.1 ± 0.5	479 ± 18
After tail cuts	824	710 ± 6	20.4 ± 0.3	158 ± 1	500 ± 3	3.3 ± 0.1	28.5 ± 4.6
After final DA cut	112	106 ± 2	17.0 ± 0.3	47.5 ± 1.1	39.2 ± 0.7	0.5 ± 0.05	1.5 ± 1.0

Table 4: $\nu\bar{\nu}q\bar{q}$ channel: Data and simulation rates after different steps of the analysis (see the description in the text). The uncertainties result from the limited simulation statistics. The CC 4-f background refers to charged-current four-fermion processes such as W^+W^- .

full event energy is reconstructed most of the time, the selection of $ZZ \rightarrow \nu\bar{\nu}q\bar{q}$ events exploits the large missing energy characteristic of this channel, and is hence sensitive to the description of the low energy tail in the reconstruction of background processes such as $q\bar{q}(\gamma)$. To study such effects and evaluate their propagation to the final steps of the analysis, large statistics samples of Z events, collected in the same conditions as the high energy data, were compared to the simulation to estimate corrections to the particle flow, in bins of momentum, polar angle and particle type. These consisted mainly of changes in multiplicities, to account for observed efficiency losses and possible duplication effects in the pattern recognition. The corrections, typically of one to a few percent in the barrel and endcaps respectively, were largest in the case of neutral particles and for high reconstructed momenta, and resulted in significantly improved agreement between data and simulation for energy flow observables such as the total charged and neutral energies, or the visible mass, including in the tails of these distributions. This procedure was then applied to all simulated high energy samples. The distribution of the discriminating variable obtained at 188.6 GeV after applying these corrections is shown in Figure 4b. The main effect was to increase the $q\bar{q}(\gamma)$ background, by up to 15%. The ZZ cross-section fit was then repeated using this modified version of the simulation and differences were used as a conservative measure of the impact of uncertainties in the description of the low energy tail of the reconstruction. To reduce effects, regions where the $q\bar{q}(\gamma)$ background dominated were removed by a final cut on the discriminating variable at zero (indicated by an arrow in Figure 4). Above this cut, 22 events remained at 182.6 GeV and 112 events at 188.6 GeV. The systematic shift in the cross-section obtained amounted to 30% relative to the expected value, and was used to represent the systematic error at both energies.

7 Four-lepton final states

About 1% of all ZZ events lead to the $l^+l^-l^+l^-$ final state. The event topology is clean and the only significant background comes from non-resonant $e^+e^-l^+l^-$ production. Events were selected if they contained between 4 and 8 charged particles, accompanied by at most 10 neutral particles, irrespective of particle identification. In order to take into account final state radiation and bremsstrahlung effects for candidate electrons, the momenta of the charged particles were rescaled if the measured sum of energies of

electromagnetic clusters in a narrow cone around the track direction was larger than the energy inferred from the track momentum measurement. The total invariant mass of the charged particles had to be greater than $50 \text{ GeV}/c^2$, and the minimum invariant mass after discarding any one of the charged particles larger than $20 \text{ GeV}/c^2$. All combinations of four charged particles with total charge zero were then examined, and a combination was selected if:

- all four tracks had their impact parameters at the interaction point smaller than 3.0 and 0.5 cm, respectively in the projections containing the beam axis and perpendicular to it, and polar angles between 10° and 170° ,
- at least three of the four charged particles had momenta greater than $5 \text{ GeV}/c$, and the least energetic particle a momentum greater than $2 \text{ GeV}/c$,
- a system of two oppositely charged particles was found with both their invariant and recoil masses within $10 \text{ GeV}/c^2$ of the Z boson mass and having the same flavour (when both were identified as either electrons or muons),
- the two particles complementary to this system were separated by at least 90° from each other,
- the invariant mass of all pairs of oppositely charged particles in the event exceeded $2 \text{ GeV}/c^2$.

At 182.6 GeV , no event was found, where predicted signal and background of respectively 0.098 ± 0.005 and 0.041 ± 0.103 events are expected. At 188.6 GeV one event was observed, where predicted signal and background of respectively 0.683 ± 0.022 and 0.076 ± 0.043 events are expected. The efficiencies of the selection were respectively 0.31 ± 0.03 and 0.41 ± 0.02 at each energy.

To study potential systematic effects arising from the method based on mass windows used to disentangle the NC02 contribution from other non-resonant four fermion processes, the results were checked with a different signal definition, consisting of generating two $l^+l^-l^+l^-$ samples, the first using NC02 graphs only and the second using all other tree-level graphs, with NC02 excluded. The first sample was used to define the signal and the second was used to estimate the background from other four-fermion processes. Results obtained in this way were fully consistent with those obtained using the mass window method.

8 Two isolated leptons with missing energy

Events from $ZZ \rightarrow \nu\bar{\nu}\mu^+\mu^-, \nu\bar{\nu}e^+e^-$ processes are characterized by two relatively acollinear charged leptons of the same flavour, with both invariant and recoil masses close to that of the Z , and by large missing energy. Although it has different production kinematics, the WW process also contributes to these final states with a large cross-section. A significant fraction of the corresponding events have exactly the same features and constitute a dominant background.

To ensure good reconstruction, tracks were required to have impact parameters at the interaction point smaller than 3.0 and 0.5 cm, respectively in the projections containing the beam axis and perpendicular to it, and polar angles between 20° and 160° . As for the $l^+l^-l^+l^-$ channel, final state radiation and bremsstrahlung effects for candidate electrons were taken into account by rescaling the momenta of the charged particles if the measured sum of energies of electromagnetic clusters in a narrow cone around the track direction was larger than the energy inferred from the track momentum measurement. Events with two particles identified as e^+e^- or $\mu^+\mu^-$ were selected if their total energy was less than

60% of that of the centre-of-mass, if the angle between them was in the range 140° - 170° , if the polar angle of the missing momentum vector was between 25° and 155° , and if the reconstructed invariant masses satisfied:

$$\min\{|M_Z - m(l^+l^-)|, |M_Z - m_{recoil}(l^+l^-)|\} < 4 \text{ GeV}/c^2, \text{ and} \\ \max\{|M_Z - m(l^+l^-)|, |M_Z - m_{recoil}(l^+l^-)|\} < 8 \text{ GeV}/c^2,$$

where $m_{recoil}(l^+l^-)$ is the invariant mass recoiling against the l^+l^- pair.

At 182.6 GeV, no event was found, with predicted signal and background of 0.109 ± 0.007 and 0.348 ± 0.155 events respectively. At 188.6 GeV, two events were observed, with predicted signal and background of 0.839 ± 0.028 and 1.025 ± 0.263 events respectively. The efficiencies of the selection were 0.26 ± 0.02 and 0.30 ± 0.02 at each energy respectively.

The main systematic effects in this channel were from uncertainties in the lepton identification efficiencies, both of which are at the few per cent level, and to a lesser extent from uncertainties in the WW cross-section used. In view of the limited statistics in this channel, these effects were neglected.

9 Combined NC02 cross-section

The cross-sections in the $q\bar{q}q\bar{q}$ and $\nu\bar{\nu}q\bar{q}$ channels were determined individually by means of binned maximum likelihood fits to the distributions of the combined variable defined in each of the corresponding analyses. To derive a combined value for the NC02 cross-section from all the six channels analysed, a global likelihood was constructed by combining the likelihoods from the fits performed in these two channels with the Poisson probabilities for observing the number of events seen in the four other channels ($\mu^+\mu^-q\bar{q}$, $e^+e^-q\bar{q}$, $l^+l^-l^+l^-$, and $\nu\bar{\nu}l^+l^-$), given the predicted numbers. This global likelihood was then maximised with respect to variations of the value of the NC02 cross-section, assuming branching ratios of the Z fixed to those expected in the Standard Model, and taking into account the scaling factors listed in table 1.

The impact of the systematic uncertainties affecting the different final states was studied by repeating the fits with modified assumptions on backgrounds and efficiencies (see the corresponding sections). Statistical errors exceeded the estimated systematic ones in each of the channels taken separately. To estimate the total systematic error on the combined result, the different uncertainties were assumed, conservatively, to be correlated, and their effects were added. This resulted in a total error of $\pm 11\%$ relative to the expected value, dominated by the uncertainty in the $\nu\bar{\nu}q\bar{q}$ channel.

The values for the NC02 cross-sections obtained were:

$$\sigma_{NC02}(182.6 \text{ GeV}) = 0.38 \pm 0.18 \text{ (stat)} \pm 0.04 \text{ (syst)} \text{ pb},$$

$$\sigma_{NC02}(188.6 \text{ GeV}) = 0.60 \pm 0.13 \text{ (stat)} \pm 0.07 \text{ (syst)} \text{ pb}.$$

These values are consistent with the Standard Model expectations of 0.25 pb and 0.65 pb at each energy, respectively, predicted by EXCALIBUR. The agreement is illustrated in Figure 5. Measurements of on-shell ZZ production by the three other LEP collaborations can be found in [21–23].

Acknowledgements

We are greatly indebted to our technical collaborators, to the members of the CERN-SL Division for the excellent performance of the LEP collider, and to the funding agencies

for their support in building and operating the DELPHI detector.
 We acknowledge in particular the support of
 Austrian Federal Ministry of Science and Traffics, GZ 616.364/2-III/2a/98,
 FNRS-FWO, Flanders Institute to encourage scientific and technological research in the
 industry (IWT), Belgium,
 FINEP, CNPq, CAPES, FUJB and FAPERJ, Brazil,
 Czech Ministry of Industry and Trade, GA CR 202/96/0450 and GA AVCR A1010521,
 Danish Natural Research Council,
 Commission of the European Communities (DG XII),
 Direction des Sciences de la Matière, CEA, France,
 Bundesministerium für Bildung, Wissenschaft, Forschung und Technologie, Germany,
 General Secretariat for Research and Technology, Greece,
 National Science Foundation (NSF) and Foundation for Research on Matter (FOM),
 The Netherlands,
 Norwegian Research Council,
 State Committee for Scientific Research, Poland, 2P03B06015, 2P03B11116 and
 SPUB/P03/DZ3/99,
 JNICT-Junta Nacional de Investigação Científica e Tecnológica, Portugal,
 Vedecka grantova agentura MS SR, Slovakia, Nr. 95/5195/134,
 Ministry of Science and Technology of the Republic of Slovenia,
 CICYT, Spain, AEN96-1661 and AEN96-1681,
 The Swedish Natural Science Research Council,
 Particle Physics and Astronomy Research Council, UK,
 Department of Energy, USA, DE-FG02-94ER40817,

References

- [1] Proceedings of the 29th International Conference on High Energy Physics, Vancouver, B.C., Canada, July 23-29 1998, eds. A.Astbury, D.Axen, J.Robinson, World Scientific 1999, talk by Michael Kobel, *Single and Pair Production of Neutral Electroweak Gauge Bosons*, page 454.
- [2] D. Chang, W-Y Keung and P.B. Pal, Phys. Rev. **D51** (1995) 1326.
- [3] K. Agashe and N.G. Deshpande, Phys. Lett **B456** (1999) 60.
- [4] K. Hagiwara, R.D. Peccei, D. Zeppenfeld and K. Hikasa, Nucl. Phys. **B282** (1987) 253.
- [5] DELPHI collaboration, P.Abreu *et al.*, Eur. Phys. J. **C10** (1999) 563.
- [6] DELPHI Collaboration, P.Aarnio *et al.*, Nucl. Instr. and Meth. **A303** (1991) 233.
- [7] DELPHI Collaboration, P.Abreu *et al.*, Nucl. Instr. and Meth. **A378** (1996) 57.
- [8] P. Chochula *et al.*, Nucl. Instr. and Meth. **A412** (1998) 304.
- [9] F.A. Berends, R. Pittau, and R. Kleiss, Comp. Phys. Comm. **85** (1995) 437; see also *Physics at LEP2* G. Altarelli, T. Sjöstrand and F. Zwirner (eds.) CERN 96-01 (1996) Vol. 2, 23.
- [10] T. Sjöstrand, Comp. Phys. Comm. **39** (1986) 347; T. Sjöstrand, *PYTHIA 5.6 and JETSET 7.3*, CERN-TH/6488-92; see also *Physics at LEP2* G. Altarelli, T. Sjöstrand and F. Zwirner (eds.) CERN 96-01 (1996) Vol. 2, 41.
- [11] Y. Kurihara *et al.*, in *Physics at LEP2* G. Altarelli, T. Sjöstrand and F. Zwirner (eds.) CERN 96-01 (1996) Vol. 2, 30.

- [12] S. Jadach, B.F.L. Ward, Z. Was, Comp. Phys Comm. **124** (2000) 233; see also S. Jadach, B.F.L. Ward, Z. Was, Comp. Phys Comm. **79** (1994) 503.
- [13] S. Jadach, W. Placzek, B.F.L. Ward, Phys. Lett **B390** (1997) 298.
- [14] T. Alderweireld *et al.*, CERN-OPEN-2000-141.
- [15] F. A. Berends, P. H. Daverveldt, R. Kleiss, Comp. Phys. Comm. **40** (1986) 271, 285 and 309.
- [16] DELPHI Collaboration, P. Abreu *et al.*, Phys. Lett **B462** (1999) 410.
- [17] G.Borisov, Nucl. Instr. Meth. **A417** (1998) 384.
- [18] see section 5.2 in DELPHI Collaboration, P. Abreu *et al.*, Eur. Phys. J. **C2** (1998) 581.
- [19] A. Ballestrero *et al.*, *Report of the QCD Working Group*, hep-ph/0006259; also published in *Reports of the working groups on precision calculations for LEP2 Physics* S. Jadach, G. Passarino, R. Pittau (eds.) CERN 2000-009 (2000), 137.
- [20] T.G.M. Malmgren, Comp. Phys. Comm. **106** (1997) 230;
T.G.M. Malmgren and K.E. Johansson, Nucl. Inst. Meth. **403** (1998) 481.
- [21] L3 Collaboration, M. Acciarri *et al.*, Phys. Lett. **B465** (1999) 363.
- [22] ALEPH Collaboration, R. Barate *et al.*, Phys. Lett. **B469** (1999) 287.
- [23] OPAL Collaboration, G. Abbiendi *et al.*, Phys. Lett. **B476** (2000) 256.
- [24] S. Jadach, W. Placzek, B.F.L. Ward, Phys. Rev. **D56** (1997) 6939.

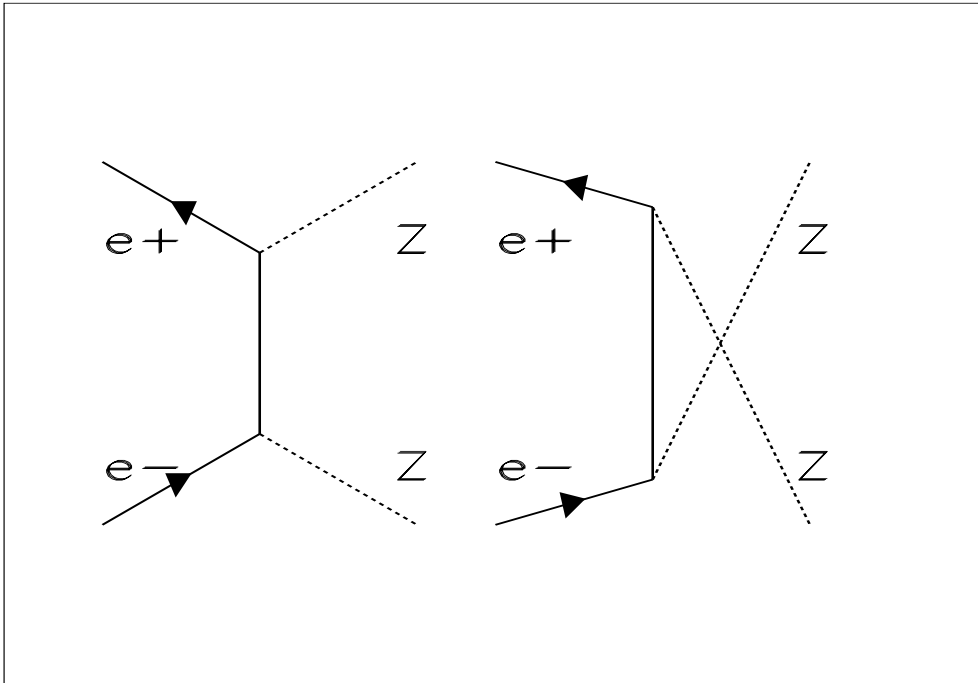


Figure 1: The Feynman graphs for on-shell ZZ production (referred to as the NC02 graphs)

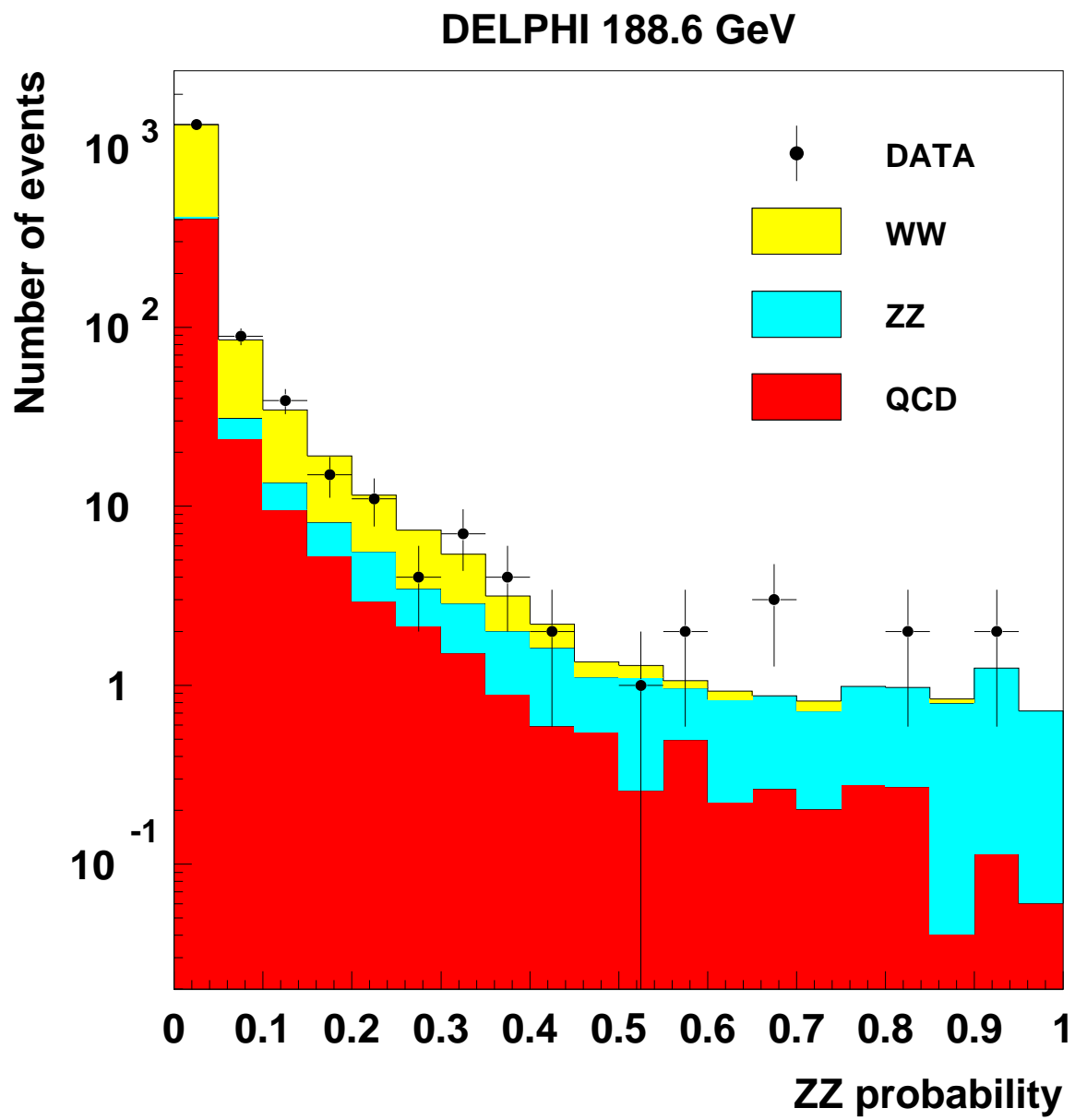


Figure 2: Distribution of the ZZ probability for all events at 188.6 GeV in the four-jet channel

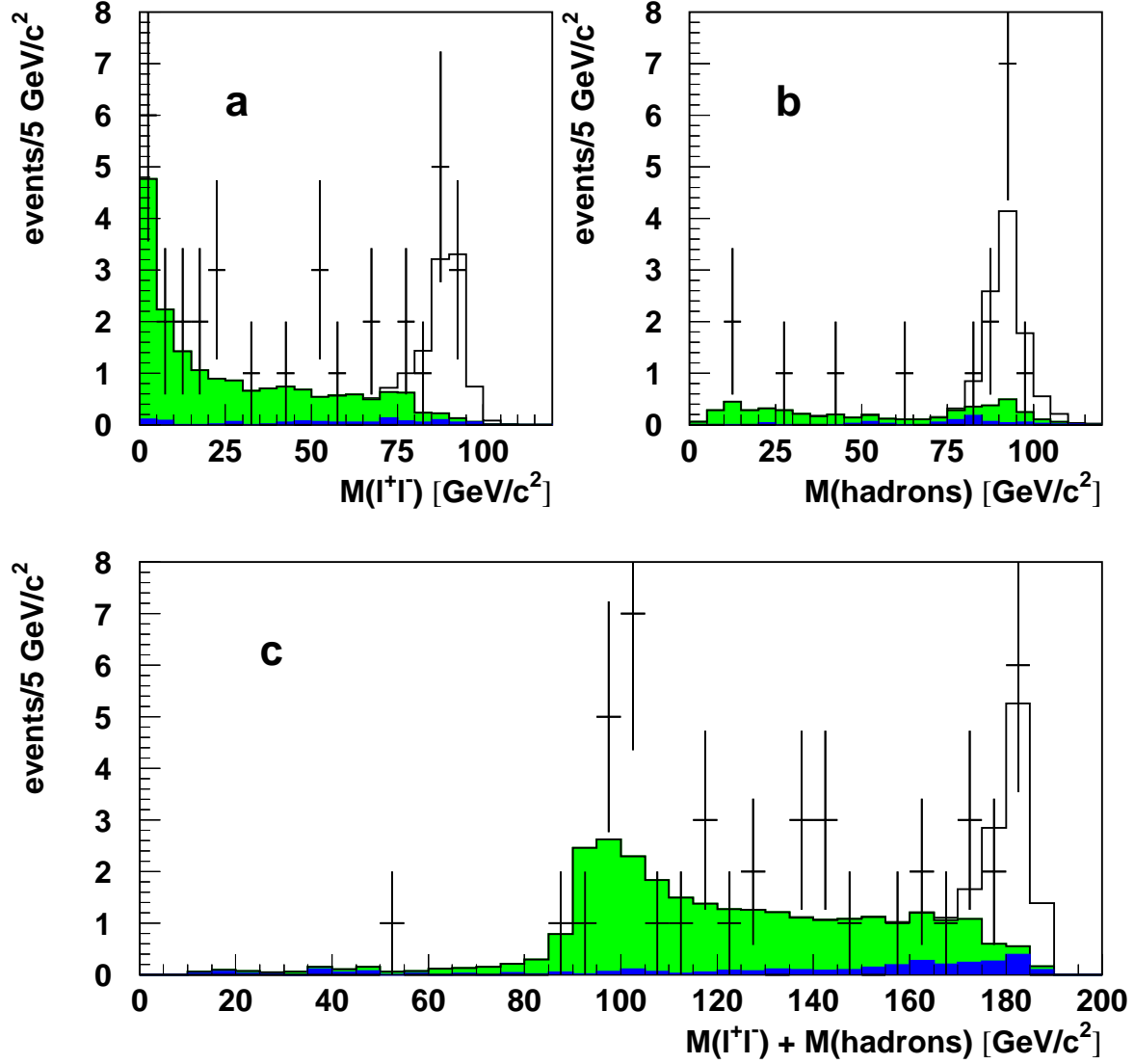
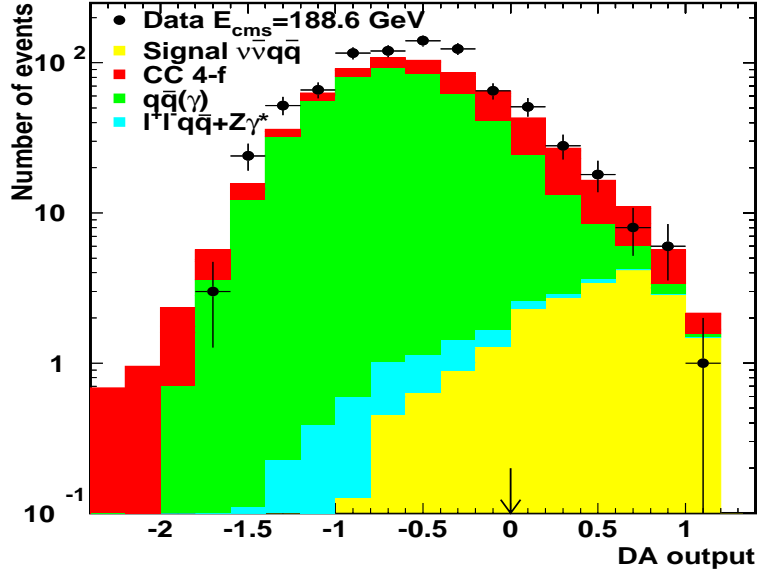


Figure 3: a) the distribution of the mass of the l^+l^- pair when the mass of the hadron system is within 15 GeV/c^2 of the nominal Z mass; b) the distribution of the mass of the hadron system when the mass of the l^+l^- pair is within 15 GeV/c^2 of the nominal Z mass; c) the distribution of the sum of the masses of the l^+l^- pair and of the hadron system. The points are the data taken at 182.6 GeV and at 188.6 GeV, and the histogram is the simulation prediction. The contribution from the signal, as defined in section 3, is indicated by the empty histogram. The contributions from backgrounds are indicated with light grey when arising from $l^+l^- q\bar{q}$ final states, and with dark filling otherwise.

a)



b)

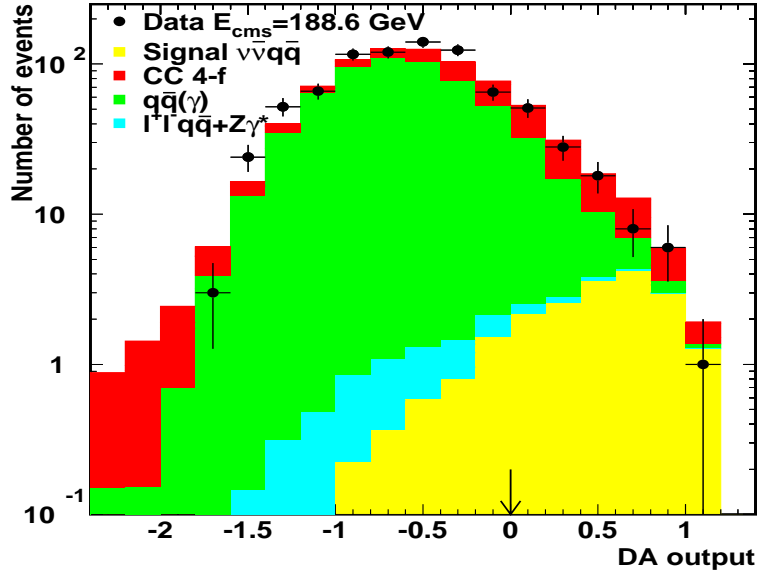


Figure 4: $\nu\bar{\nu}q\bar{q}$ channel: The second-order discriminant for the data at 188.6 GeV, for the expected signal (light) and for the backgrounds from $l^+l^-q\bar{q}$ and $Z\gamma^*$ (light grey), $q\bar{q}(\gamma)$ (dark grey) and $W e \nu_e$ and WW (dark, CC 4-f in the legend) processes are shown, using the nominal (plot a) and corrected (plot b) simulation, following the procedure described in the text. The main effect from the correction procedure was to increase the $q\bar{q}(\gamma)$ background component. The arrow indicates the cut used to remove the part of the distribution where the $q\bar{q}(\gamma)$ background dominates, in order to reduce the systematic error as described in the text.

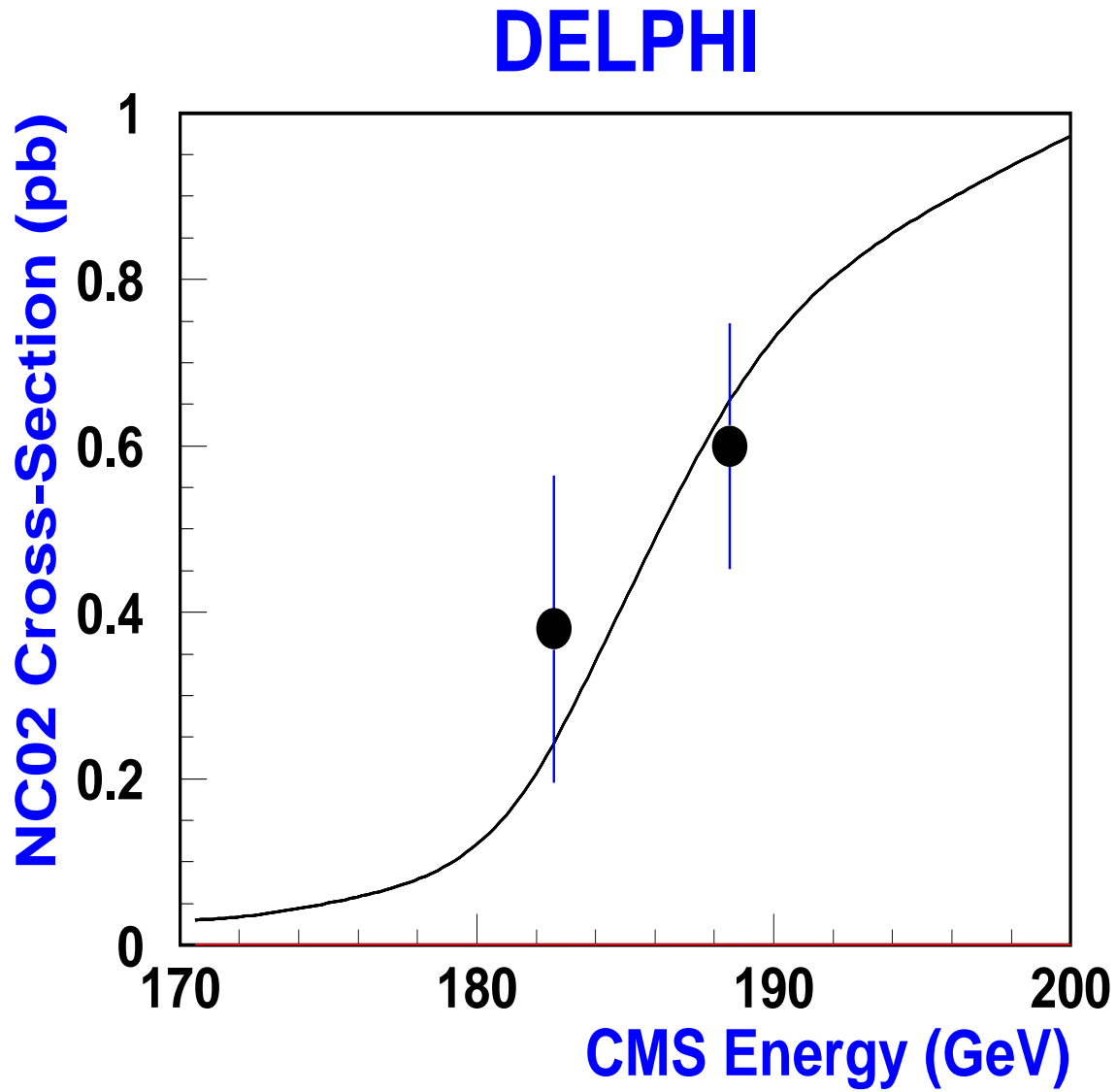


Figure 5: Combined NC02 cross-sections measured from data collected in 1997 and 1998. The solid curve was computed using the YFSZZ Monte-Carlo [24]. Values obtained with the EXCALIBUR Monte-Carlo were within $\pm 1\%$ of those obtained with YFSZZ.